ChemComm

Chemical Communications

rsc.li/chemcomm

ROYAL SOCIETY
OF CHEMISTRY

COMMUNICATION
Zhichao Pei *et al.*
Pillar[5]arene-based supramolecular photosensitizer for
enhanced hypoxic-tumor therapeutic effectiveness

ChemComm

Check for updates

Pillar[5]arene-based supramolecular photosensitizer for enhanced hypoxic-tumor therapeutic effectiveness†

Shuang Chao,‡ Ziyan Shen,‡ Yuxin Pei, [ID] Yinghua Lv, Xiaolin Chen, Jiaming Ren, Ke Yang and Zhichao Pei [ID] *

A galactose-targeting supramolecular photosensitizer system DOX@ GP5⊃NBSPD was constructed based on a host–guest inclusion complex. The supramolecular system could achieve efficient delivery of DOX/NBS and selective release under GSH stimulation. *In vitro* studies revealed that this supramolecular DOX/NBS co-delivery system exhibited high ROS production and excellent cancer cell damage capability in a hypoxic environment. This strategy can therefore achieve enhanced hypoxic-tumor therapeutic effectiveness by chemo-photodynamic combination.

Supramolecular chemistry has developed rapidly and attracted extensive attention from the scientific community since the 1970s.[1] In recent years, benefiting from the excellent supramolecular interaction properties, supramolecular-assembly-based platforms have stood out from many tumor diagnosis and treatment strategies.[2–5] An increasing number of macrocyclic hosts including cyclodextrins,[6] calix[*n*]arenes,[7] cucurbit[*n*]urils,[8] and pillar[*n*]arenes[9] have been introduced to construct functional supramolecular systems for targeted therapy of tumors. Photodynamic therapy (PDT), an effective cancer treatment method, relies on the generation of reactive oxygen species (ROS) by photosensitizers (PSs) and light to damage cancer cells.[10,11] However, the development of PSs is limited due to its lack of targeting capability, poor solubility/stability, and dark toxicity.[12,13] Supramolecular PDT systems based on host–guest interaction provide innovative strategies to effectively overcome the limitations of PDT. Increasing numbers of PDT systems based on supramolecular structures have been reported successively.[14–16]

In most cases, the light-activated PSs, *via* a type II mechanism, transform triplet ground state molecular oxygen ($^3O_2$)

into its highly reactive singlet oxygen ($^1O_2$). These PDT systems based on the type II mechanism are highly dependent on the O_2 concentration of the tumor tissues.[17–19] However, the hypoxic tumor microenvironment ($pO_2 < 5$ mmHg), due to malignant proliferation of tumors and insufficient blood supply, weakens the efficacy of O_2-dependent PDT.[20,21] Therefore, developing advanced methods and materials for hypoxic-tumor PDT is of great significance for cancer treatment. In the past few years, many strategies have been developed to improve the PDT efficacy of hypoxic tumors, where the approaches mainly include the following methods: increasing O_2 concentration through direct or indirect O_2 supplying strategies, reducing the dependence on O_2 by using the novel PDT paradigms, and combining PDT with other therapeutic forms that are O_2-independent or hypoxia-activated.[22,23] Among them, some light-activated PSs could achieve the production of $O_2^{-\bullet}$ through transfer of electrons or a hydrogen atom from substrates *via* a type I reaction mechanism. Then, $O_2^{-\bullet}$ could be catalyzed by SOD (superoxide dismutase) to produce H_2O_2, which is further catalyzed through a Fenton reaction to produce highly toxic $OH^\bullet$. This process greatly reduces the dependence on O_2 concentration.[24] According to reports, a Nile blue analog, which is modified by a ''heavy atom'', has excellent photocatalytic properties to generate $O_2^{-\bullet}$ *via* a type I reaction mechanism in hypoxic-tumor PDT.[24,25] However, there is no report on a supramolecular PDT system for PDT of hypoxic tumors. Therefore, it is of great scientific significance to design a supramolecular PDT system that can improve the PDT efficacy of hypoxic tumors.

Herein, we report for the first time the construction of a supramolecular photosensitizer system for hypoxic-tumor PDT based on host–guest interaction between a galactose functionalized pillar[5]arene (GP5) and Nile blue pyridine derivative which was modified with sulfur atoms (NBSPD).[26–28] As shown in Scheme 1, the amphiphilic supramolecular photosensitizer (GP5⊃NBSPD) can be successfully obtained and self-assembled into nano-vesicles. Chemo-photodynamic combined therapy has attracted much attention due to its excellent

Shaanxi Key Laboratory of Natural Products & Chemical Biology, College of Chemistry & Pharmacy, Northwest A&F University, Yangling 712100, P. R. China. E-mail: peizc@nwafu.edu.cn; Fax: +86-29-8709-2769; Tel: +86-29-8709-2769
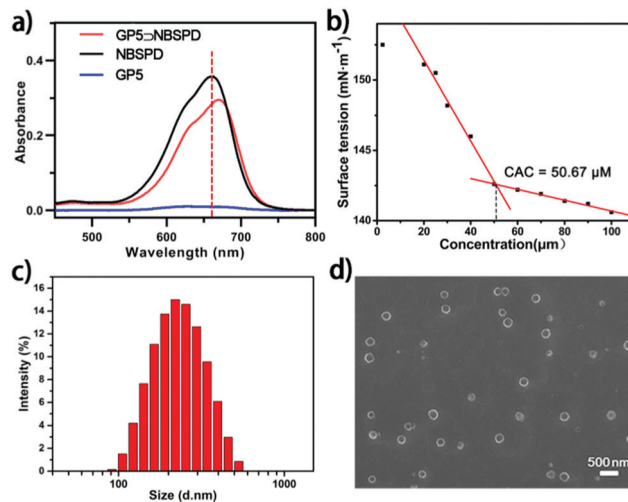
‡ These authors contributed equally.
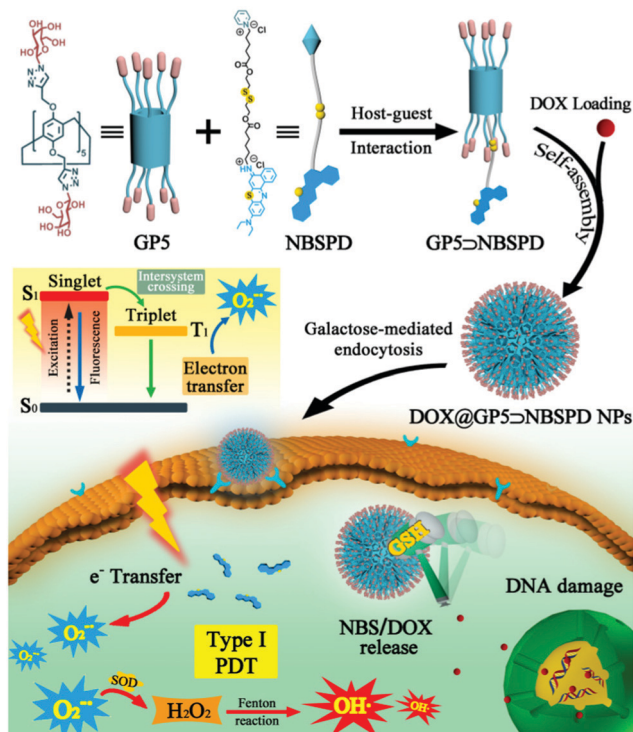
Scheme 1 Schematic illustration of the construction of the supramole-cular photosensitizer (GP5⊃NBSPD) and its application in targeted drug delivery and hypoxic-tumor PDT.

Fig. 1 (a) UV-vis spectra of NBSPD, GP5 and GP5⊃NBSPD; (b) CAC of GP5⊃NBSPD NPs; (c) DLS of GP5⊃NBSPD NPs; (d) SEM image of GP5⊃NBSPD NPs.

anticancer activity. In this work, Doxorubicin hydrochloride (DOX) as a model anticancer drug was loaded to prepare DOX@ GP5⊃NBSPD nanoparticles (NPs). The DOX@GP5⊃NBSPD NPs could target HepG2 (human hepatoma cells) through specific recognition between galactose and asialoglycoprotein receptor (ASGR) over-expressed on the cell membrane.[29] DOX and NBS can be released rapidly in cancer cells by cleavage of disulfide bonds at high concentrations of GSH. Finally, cancer cells were damaged by combining DOX with ROS ($O_2^{-\bullet}$, H_2O_2, and highly toxic $OH^{\bullet}$) which were produced through a type I reaction mechanism by photocatalytic NBS in a hypoxic microenvironment. The chemo-photodynamic combination could achieve enhanced hypoxic-tumor therapeutic effectiveness.

GP5 and NBSPD were synthesized according to the reported method, respectively (Schemes S1 and S2, ESI†).[29,30] The chemical structures of the synthesized compounds were characterized via ^{1}H NMR, ^{13}C NMR, and HRMS (Fig. S1–S14, ESI†). The host–guest complexation of GP5 and NBSPD was proven by ^{1}H NMR spectroscopy in D_2O (Fig. S15, ESI†). It was observed that the pyridinium group of NBSPD had a prominent upfield chemical shift by the inclusion-induced shielding effect. The binding stoichiometry between GP5 and NBSPD was 1:1, measured by the Job's plot method (Fig. S16, ESI†). On the basis of the ITC (isothermal titration calorimetry) data (Fig. S17, ESI†), K_a for the GP5⊃NBSPD host–guest complex was calculated to be 1.868×10^5 M^{-1},[31] which indicated a strong binding affinity between GP5 and NBSPD. Furthermore, as shown in Fig. 1a, a red-shift was observed from UV-vis

absorption spectroscopy due to electronic interactions between GP5 and NBSPD, further revealing the formation of a stable host–guest complex. After establishing the GP5⊃NBSPD recognition motif in water, the amphiphilic supramolecular photosensitizers were used to construct stable nanoparticles. As shown in Fig. 1b, the critical aggregation concentration (CAC) of GP5⊃NBSPD NPs was calculated to be 50.67 μM by measuring the optical transmittance of the nanoparticle solution. The obvious Tyndall effect demonstrated the formation of GP5⊃NBSPD NPs (Fig. S18, ESI†). Moreover, the assembled morphology and size of the GP5⊃NBSPD NPs were characterized by DLS, SEM and TEM, respectively. The DLS results indicated that the mean diameter of the GP5⊃NBSPD NPs was *ca.* 230 nm (Fig. 1c). Spherical NPs with a mean diameter of *ca.* 220 nm were observed by SEM (Fig. 1d). GP5⊃NBSPD NPs could be identified as vesicles by TEM (Fig. S18, ESI†). The different experimental results were caused by diverse experimental conditions (a solid state under vacuum for SEM and TEM as opposed to an aqueous solution for DLS).

Furthermore, both NBSPD and GP5⊃NBSPD displayed an intense absorption profile at 600–700 nm (Fig. 1a), promising less phototoxicity and deeper permeability to normal organisms. As shown in Fig. 2a, fairly high NIR fluorescence was exhibited after 660 nm excitation. However, the emission fluorescence value of NBSPD was much higher than that of GP5⊃NBSPD. This phenomenon may be mainly due to the aggregation-caused quenching (ACQ) of NBS in GP5⊃NBSPD NPs (Fig. S19, ESI†).[32] Thereafter, we determined the ROS generation of the GP5⊃NBSPD NPs. $O_2^{-\bullet}$ probe dihydrorhodamine 123 (DHR123) was used to confirm $O_2^{-\bullet}$ production.[24] As shown in Fig. S19 and Fig. 2b, c, both NBSPD and GP5⊃NBSPD showed good $O_2^{-\bullet}$ production. Vitamin C-Na (VcNa) was added into NBSPD solution as a scavenger to prove that the enhanced DHR123 signal was caused by $O_2^{-\bullet}$. The results showed that the addition of VcNa significantly reduced the concentration of $O_2^{-\bullet}$. Meanwhile, $OH^{\bullet}$ and $^1O_2$
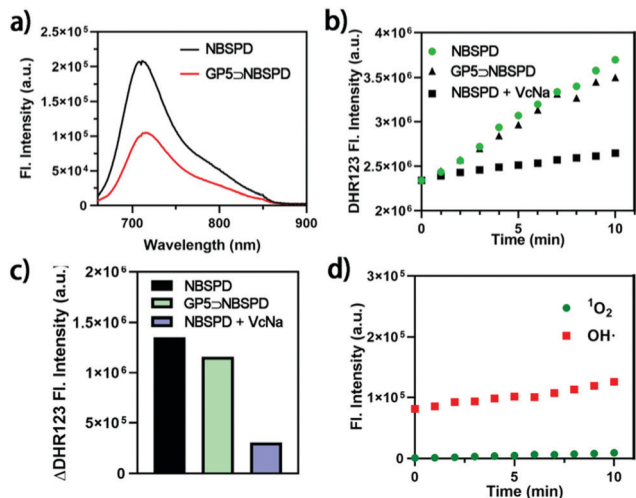
Fig. 2 (a) Fluorescence spectra of NBSPD and GP5⊃NBSPD; (b and c) fluorescence intensity of DHR123 at 526 nm after 630 nm irradiation for 10 min; (d) fluorescence intensity of HPF at 516 nm and SOSG at 525 nm as the specific indicators for OH• and $^1O_2$ after 630 nm irradiation for 10 min.

Fig. 3 (a) Schematic illustration of DHE for $O_2^{-\bullet}$ detection; (b and c) CLSM images of intracellular light dose-dependent $O_2^{-\bullet}$ generation of GP5⊃NBSPD NPs in HepG2 cells determined by DHE staining: 660 nm light source, 0–15 J cm^{-2}; (d) ROS detection in HepG2 cells after exposure to 630 nm light with 15 J cm^{-2} under normoxia and hypoxia conditions using DHE, HPF, and SOSG as the $O_2^{-\bullet}$, OH•, and $^1O_2$ fluorescence indicator, respectively. The scale bar is 20 μm.

were almost undetected when we employed hydroxyphenyl fluorescein (HPF) and singlet oxygen sensor green (SOSG) as the specific indicators for OH• and $^1O_2$, respectively (Fig. 2d and Fig. S20, ESI†). These results indicated that the supramolecular photosensitizer mainly produces ROS through a type I reaction mechanism, which lays a solid foundation for their application in improving the effect of hypoxic-tumor PDT.

To further investigate the $O_2^{-\bullet}$ generation of the supramolecular photosensitizer GP5⊃NBSPD in cells, a droethidium (DHE) staining assay was employed. As shown in Fig. 3a, DHE could be oxidized to ethidium by $O_2^{-\bullet}$, which intercalates into DNA and glows with a bright red fluorescence. In the normoxic environment, after exposure to 630 nm light, an increase in average fluorescence intensity was observed by confocal laser scanning microscope (CLSM) as the light dose increased from 0 to 15 J cm^{-2} in HepG2 cells. Meanwhile, the red fluorescence decreased rapidly when VcNa was added as an $O_2^{-\bullet}$ scavenger (Fig. 3b and c). Additionally, the liquid paraffin covering method was used to simulate the tumor hypoxic environment to further study the effect of a supramolecular photosensitizer in a hypoxic environment. The cells were covered with sterilizing liquid paraffin for 12 h, and the anaerobic indicator ROS-ID was used to prove intracellular hypoxia. The experimental results show that this is an effective method to mimic the hypoxic environment of tumors (Fig. S21, ESI†). Encouragingly, clear red fluorescence of ethidium was observed in a hypoxic environment despite it being weaker than in a normoxic environment (Fig. 3d). Moreover, the most toxic OH• could be detected in HepG2 cells by HPF after irradiation of 630 nm light. This is mainly due to SOD catalyzing $O_2^{-\bullet}$ to produce H_2O_2, which was further decomposed through a Fenton reaction. However, there was almost no $^1O_2$ generation observed. The main reason for this is NBS, which was modified with sulfur atoms to produce $O_2^{-\bullet}$ through a type I reaction mechanism. These results are consistent with the results of the extracellular assay.

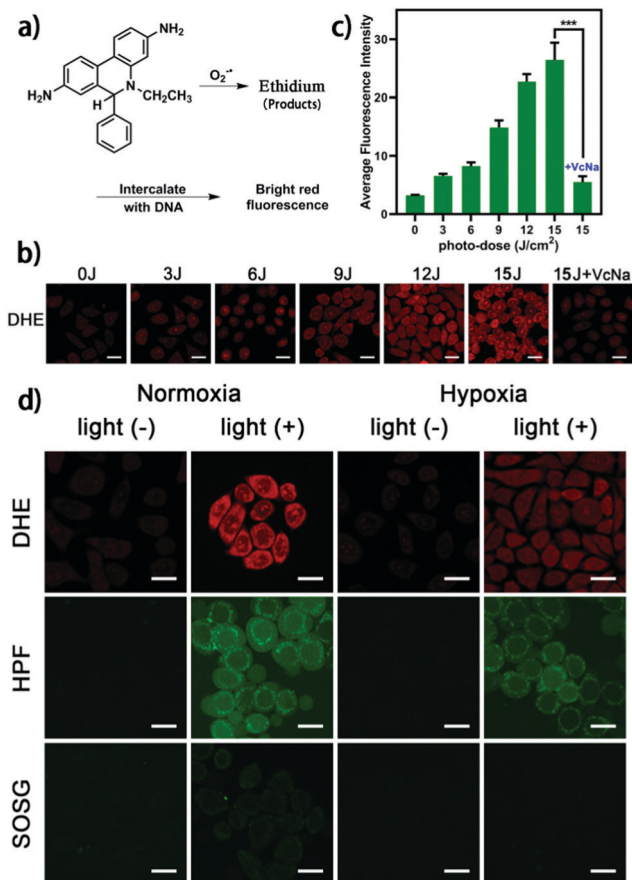Next, the targeting ability of GP5⊃NBSPD NPs was verified. As shown in Fig. S22 (ESI†), HepG2 cells showed a bright red fluorescence compared to HL7702 cells (normal human liver cells) after exposure to 630 nm light. This is due to the galactose of GP5⊃NBSPD, which can specifically recognize ASGR over-expressed on the membrane surface of HepG2 cells. DOX was loaded into the hydrophilic cavity of GP5⊃NBSPD NPs. The DOX loading capability of GP5⊃NBSPD NPs was calculated to be 29.8% (cf. standard curve in Fig. S23, ESI†) by UV-Vis spectrophotometry. Spherical DOX@GP5⊃NBSPD NPs with a mean diameter of ca. 195 nm were observed by SEM (Fig. S24, ESI†). We further investigated the GSH-responsive behaviour of the DOX@GP5⊃NBSPD NPs. The experimental result showed that 58% DOX was released from the DOX@GP5⊃NBSPD NPs rapidly within 2 h under 5 mM GSH PBS solutions. The cumulative amount of DOX released was up to 89% after 24 h (Fig. S25, ESI†). Furthermore, flow cytometry measured higher fluorescence intensity in the DOX@GP5⊃NBSPD NP treated HepG2 cells compared to the free DOX treated HepG2 cells (Fig. S26, ESI†). The fluorescence intensity of DOX decreased
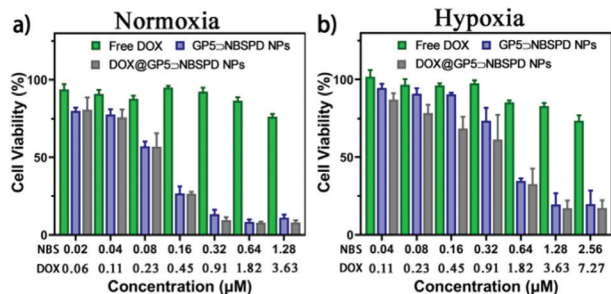
Fig. 4 *In vitro* cytotoxicity results of free DOX, GP5⊃NBSPD NPs and DOX@GP5⊃NBSPD NPs on HepG2 cells in the presence of light irradiation under normoxia (a) and hypoxia (b) conditions for 24 h.

after adding lactose acid (LBA), which inhibited the activity of ASGR. However, there was no significant difference in DOX fluorescence intensity between the DOX@GP5⊃NBSPD NP group and the free DOX group in HL7702 cells and 293T cells (healthy human embryonic kidney cells). These results indicate that GP5⊃NBSPD is a good nanocarrier for targeted drug delivery.

The methyl tetrazolium (MTT) assay was employed to demonstrate the anticancer activity of DOX@GP5⊃NBSPD NPs. First, the dark toxicity of GP5⊃NBSPD NPs was evaluated. GP5⊃NBSPD NPs showed low dark toxicity to both HepG2 cells and HL7702 cells (Fig. S27, ESI†). Upon 15 J cm^{-2} irradiation, although hypoxia slightly affected the effect of PDT, GP5⊃NBSPD NPs still caused strong cell damage (Fig. 4). Meanwhile, the DOX@GP5⊃NBSPD NP group exhibited greater cytotoxicity than the other two groups. For example, at a low DOX@GP5⊃NBSPD concentration of 1.28 μM, up to 92.2% of cancer cells were killed in a normoxic environment compared to 83.0% in a hypoxic environment. This result indicated that the supramolecular photosensitizer GP5⊃NBSPD is an excellent nanocarrier with high potential for targeted drug delivery and hypoxic-tumor PDT.

In summary, a novel amphiphilic supramolecular photosensitizer GP5⊃NBSPD was constructed based on the host–guest complexation of galactose functionalized pillar[5]arene (GP5) and Nile blue pyridine derivative (NBSPD). GP5⊃NBSPD can self-assemble into nano-vesicles and be loaded with DOX to form DOX@GP5⊃NBSPD NPs. *In vitro* studies showed that DOX@GP5⊃NBSPD NPs can achieve efficient delivery of DOX/NBS by galactose recognizing HepG2 cells and selective release under GSH stimulation. This supramolecular DOX/NBS co-delivery system exhibited high ROS production and excellent cancer cell damage capability in a hypoxic environment. Therefore, the chemo-photodynamic combination platform based on the pillar[5]arene-based supramolecular photosensitizer has provided a great strategy for enhanced hypoxic-tumor therapeutic effectiveness.

Conflicts of interest

There are no conflicts to declare.

Notes and references

1 J.-M. Lehn, *Angew. Chem., Int. Ed. Engl.*, 1988, **27**, 89–112.
2 Y. Chang, K. Yang, P. Wei, S. Huang, Y. Pei, W. Zhao and Z. Pei, *Angew. Chem., Int. Ed.*, 2014, **53**, 13126–13130.
3 X.-Y. Hu, L. Gao, S. Mosel, M. Ehlers, E. Zellermann, H. Jiang, S. K. Knauer, L. Wang and C. Schmuck, *Small*, 2018, **14**, 1803952.
4 L. Chen, Y. Chen, Y. Zhang and Y. Liu, *Angew. Chem., Int. Ed.*, 2021, **60**, 7654–7658.
5 Z. Li, N. Song and Y.-W. Yang, *Matter*, 2019, **1**, 345–368.
6 F. Schibilla, A. Holthenrich, B. Song, A. L. L. Matos, D. Grill, D. R. Martir, V. Gerke, E. Z. Colman and B. J. Ravoo, *Chem. Sci.*, 2018, **9**, 7822–7828.
7 C. Tu, L. Zhu, P. Li, Y. Chen, Y. Su, D. Yan, X. Zhu and G. Zhou, *Chem. Commun.*, 2011, **47**, 6063–6065.
8 M. Gupta, K. Parvathi, S. Mula, D. K. Maity and A. K. Ray, *Photochem. Photobiol. Sci.*, 2017, **16**, 499–506.
9 K. Yang, J. Wen, S. Chao, J. Liu, K. Yang, Y. Pei and Z. Pei, *Chem. Commun.*, 2018, **54**, 5911–5914.
10 J. Ge, M. Lan, B. Zhou, W. Liu, L. Guo, H. Wang, Q. Jia, G. Niu, X. Huang, H. Zhou, X. Meng, P. Wang, C.-S. Lee, W. Zhang and X. Han, *Nat. Commun.*, 2014, **5**, 4596.
11 S. Monro, K. L. Colón, H. Yin, J. Roque, P. Konda, S. Gujar, R. P. Thummel, L. Lilge, C. G. Cameron and S. A. McFarland, *Chem. Rev.*, 2019, **119**, 797–828.
12 H. Zhu, P. Cheng, P. Chen and K. Pu, *Biomater. Sci.*, 2018, **6**, 746–765.
13 Z. Zhou, J. Song, L. Nie and X. Chen, *Chem. Soc. Rev.*, 2016, **45**, 6597–6626.
14 D. Jia, X. Ma, Y. Lu, X. Li, S. Hou, Y. Gao, P. Xue, Y. Kang and Z. Xu, *Chin. Chem. Lett.*, 2021, **32**, 162–167.
15 K. Yang, Z. Zhang, J. Du, W. Li and Z. Pei, *Chem. Commun.*, 2020, **56**, 5865–5876.
16 X. Li, S. Lee and J. Yoon, *Chem. Soc. Rev.*, 2018, **47**, 1174–1188.
17 T. J. Dougherty, C. J. Gomer, B. W. Henderson, G. Jori, D. Kessel, M. Korbelik, J. Moan and Q. Peng, *J. Natl. Cancer Inst.*, 1998, **90**, 889–905.
18 J.-P. Wei, X.-L. Chen, X.-Y. Wang, J.-C. Li, S.-G. Shi, G. Liu and N.-F. Zheng, *Chin. Chem. Lett.*, 2017, **28**, 1290–1299.
19 X. Li, B.-D. Zheng, X.-H. Peng, S.-Z. Li, J.-W. Ying, Y. Zhao, J.-D. Huang and J. Yoon, *Coord. Chem. Rev.*, 2019, **379**, 147–160.
20 J. E. Moulder and S. Rockwell, *Cancer Metastasis Rev.*, 1987, **5**, 313–341.
21 J. M. Brown and W. R. Wilson, *Nat. Rev. Cancer*, 2004, **4**, 437–447.
22 X. Li, N. Kwon, T. Guo, Z. Liu and J. Yoon, *Angew. Chem., Int. Ed.*, 2018, **130**, 11694–11704.
23 L. Huang, S. Zhao, J. Wu, L. Yu, N. Singh, K. Yang, M. Lan, P. Wang and J. S. Kim, *Coord. Chem. Rev.*, 2021, **438**, 213888.
24 M. Li, J. Xia, R. Tian, J. Wang, J. Fan, J. Du, S. Long, X. Song, J. W. Foley and X. Peng, *J. Am. Chem. Soc.*, 2018, **140**, 14851–14859.
25 M. Li, Y. Shao, J. H. Kim, Z. Pu, X. Zhao, H. Huang, T. Xiong, Y. Kang, G. Li, K. Shao, J. Fan, J. W. Foley, J. S. Kim and X. Peng, *J. Am. Chem. Soc.*, 2020, **142**, 5380–5388.
26 T. Ogoshi, S. Kanai, S. Fujinami, T.-A. Yamagishi and Y. Nakamoto, *J. Am. Chem. Soc.*, 2008, **130**, 5022–5023.
27 L. Shao, Y. Pan, B. Hua, S. Xu, G. Yu, M. Wang, B. Liu and F. Huang, *Angew. Chem., Int. Ed.*, 2020, **59**, 11779–11783.
28 J. Chen, Y. Zhang, Y. Chai, Z. Meng, Y. Zhang, L. Chen, D. Quan, Y. Wang, Q. Meng and C. Li, *Chem. Sci.*, 2021, **12**, 5202–5208.
29 X. Wu, Y. Zhang, Y. Lu, S. Pang, K. Yang, Z. Tian, Y. Pei, Y. Qu, F. Wang and Z. Pei, *J. Mater. Chem. B*, 2017, **5**, 3483–3487.
30 S. Chao, X. Lv, N. Ma, Z. Shen, F. Zhang, Y. Pei and Z. Pei, *Chem. Commun.*, 2020, **56**, 8861–8864.
31 Y. Cao, X. Hu, Y. Li, X. Zou, S. Xiong, C. Lin, Y. Shen and L. Wang, *J. Am. Chem. Soc.*, 2014, **136**, 10762–10769.
32 B. Lozano-Torres, J. F. Blandez, I. Galiana, A. García-Fernández, M. Alfonso, M. D. Marcos, M. Orzáez, F. Sancenón and R. Martínez-Máñez, *Angew. Chem., Int. Ed.*, 2020, **59**, 15152–15156.